CORE
Metadata, citation and similar papers at core.ac.uk
Provided by ePrints@Bangalore University

Available online at www.sciencedirect.com
SCIENCE DIRECT®

Solid State Communications 136 (2005) 427–432

solid state communications

www.elsevier.com/locate/ssc

Synthesis, structural and transport properties of nanocrystalline $La_{1-x}Ba_xMnO_3$ $(0.0 \leq x \leq 0.3)$ powders

B.M Nagabhushana[a], G.T. Chandrappa[a,*], R.P. Sreekanth Chakradhar[b], K.P. Ramesh[b], C. Shivakumara[c]

[a]*Department of Chemistry, Central college, Bangalore University, Bangalore 560 001, India*
[b]*Department of Physics, Indian Institute of Science, Bangalore 560 012, India*
[c]*Solid State and Structural Chemistry Unit, Indian Institute of Science, Bangalore 560 012, India*

Received 30 March 2005; accepted 18 July 2005 by G. Luke

Available online 3 August 2005

Abstract

Nanocrystalline $La_{1-x}Ba_xMnO_3$ $(0.0 \leq x \leq 0.3)$ manganites have been prepared by a simple and instantaneous solution combustion method, which is a low temperature initiated synthetic route to obtain fine-grained powders with relatively high surface area. The phase purity and crystal structure of the combustion products are carried out by powder X-ray diffraction. The as-made nanopowders are in cubic phase. On calcination to 900 °C, barium doped manganites retain cubic phase, whereas barium free manganite transformed to rhombohedral phase. The scanning electron microscope (SEM) results revealed that the combustion-derived compounds are agglomerated with fine primary particles. The doped manganites have surface area in the range 24–44 m^2/g. The surface area of the manganites increases with barium content, whereas it decreases on calcination. Both undoped and doped lanthanum manganites show two active IR vibrational modes at 400 and 600 cm^{-1}. The low temperature resistivity measurements have been carried out by four-probe method down to 77 K. All the samples exhibit metal–insulator behaviour and metal–insulator transition temperature (T_{M-I}) in the range 184–228 K and it is interesting to note that, as the barium content increases the T_{M-I} shifts to lower temperature side. The maximum T_{M-I} of 228 K is observed for $La_{0.9}Ba_{0.1}MnO_3$ sample.
© 2005 Elsevier Ltd. All rights reserved.

PACS: 75.47.Lx; 73.43.Qt

Keywords: A. Nanocrystalline manganites; B. Combustion synthesis; D. Barium doping; D. Metal–insulator transition; D. Transport properties

1. Introduction

Nowadays, nanomaterials have attracted considerable attention because of their unique chemical, physical, electrical, magnetic, optical and mechanical properties. Because of these properties, they are useful as catalysts, sensors, coating materials and miniaturization of devices [1]. Therefore, it is of interest to investigate nanocrystalline manganites with particle sizes comparable with magnetic domain sizes in order to understand better the mechanism for the colossal magnetoresistance (CMR) properties. Observation of CMR in the hole-doped perovskite manganites of the general formula $RE_{1-x}A_xMnO_3$ (RE = rare-earth ion, A = divalent alkaline-earth metal ion) has spurred considerable interest in the study of these compounds owing to the remarkable magneto transport phenomena and the potential technological applications to new devices such as magnetic-reads, field sensors and magnetic memories [2–4]. Doping the parent compound $LaMnO_3$ with divalent alkaline-earth cation (A^{2+}) such as Ca^{2+}, Ba^{2+} and Sr^{2+} will cause the conversion of a proportional number of Mn^{3+}

* Corresponding author. Tel./fax: +91 8023523154.
E-mail address: gtchandrappa@yahoo.co.in (G.T. Chandrappa).

0038-1098/$ - see front matter © 2005 Elsevier Ltd. All rights reserved.
doi:10.1016/j.ssc.2005.07.017

to Mn^{4+}. The mixed valencies of Mn ions play a major role in double exchange (DE) mechanism [5–7]. It is believed that the DE interaction between Mn^{4+} and Mn^{3+} ion pairs is responsible for the metallic character and ferromagnetic (FM) properties in these manganese oxides.

There are many techniques for the preparation of perovskite based rare earth manganites, which include solid-state reaction [8], sol–gel [9], nitrate citrate gel-combustion [10], co-precipitation [11], acrylamide polymerization [12], hydrothermal [13], combustion [14] and microwave techniques [15]. A majority of work available on the synthesis of barium doped lanthanum manganites is generally based on high temperature ceramic method.

In the present work, we describe a simple and novel method of synthesizing nanocrystalline barium substituted lanthanum manganites by a low temperature initiated solution combustion route using oxalyl dihydrazide (ODH) as a fuel and the corresponding metal nitrates as oxidizers. Instantaneous combustion synthesis is an important powder processing technique generally used to prepare oxide ceramics [16]. It involves several advantages like fast heating rates, short reaction time ($\sim$5 min), besides producing foamy, homogeneous and high surface area nanocrystalline products. It has also the advantage of doping desired amounts of dopant ions in solution medium and 'low processing temperature' leading to uniform crystallite size at superfine dimensions. High purity and homogeneity can be achieved at temperature as low as 300 °C as against 1470 °C needed to synthesize these materials via ceramic route [17]. The combustion products are characterized by XRD, EDS, SEM, surface area and FTIR. The zero field low temperature resistivity measurements down to 77 K were carried out by four-probe method on sintered pellette samples.

2. Experimental

2.1. Chemicals

Analar grade lanthanum nitrate ($La(NO_3)_3\cdot 4H_2O$), barium nitrate ($Ba(NO_3)_2\cdot 4H_2O$) and manganese nitrate ($Mn(NO_3)_2\cdot 4H_2O$) were used as oxidizers and oxalyl dihydrazide, $C_2H_6N_4O_2$(ODH) as a fuel. ODH was prepared in our laboratory by the reaction of diethyl oxalate with hydrazine hydrate [18]. The detailed calculation of stoichiometry has been reported elsewhere [19].

2.2. Synthesis of $La_{1-x}Ba_xMnO_3$ ($0.0 \le x \le 0.3$) manganites

The aqueous solution containing metal nitrates and fuel are taken in a petri dish of approximately 300 ml capacity and excess water is allowed to evaporate by heating on a hot plate until wet powder is left out. Then the petri dish is introduced into a muffle furnace maintained at 300 °C. Initially, the wet powder undergoes dehydration followed by decomposition with large amount of gases (oxides of nitrogen and carbon). The mixture ignites and catches fire to give a voluminous combustion product. The as-formed powders are free from carbon residue. Assuming complete combustion, the general equation for the formation of samples can be proposed as follows

$$(1-x)La(NO_3)_3(aq) + xBa(NO_3)_2(aq) + Mn(NO_3)_2(aq) + C_2H_6N_4O_2(aq) \rightarrow La_{1-x}Ba_xMnO_3(S) + CO_2(g) + H_2O(g) + N_2(g)$$

The phase purity and crystal structure were examined by Scintag X-ray diffractometer using Cu K_α radiation with a nickel filter. The average crystallite sizes were determined by Debye–Scherrer's formula. The morphology of the powder was examined using JEOL (JSM-840 A) scanning electron microscope (SEM). The specific surface area of the powder samples was determined by Quanta Chrome Corporation, NOVA 1000 Gas Sorption Analyzer. FTIR spectra of the as-formed and calcined samples were performed with Perkin–Elmer–FTIR spectrometer, (spectrum 1000). The electrical resistivity measurements were carried out on sintered pellets at 900 °C for 6 h in air, using Dc four-probe method in the range 77–300 K.

3. Results and discussion

3.1. Powder X-ray diffraction

Figs. 1 and 2 show the powder X-ray diffraction patterns of as-formed and calcined (900 °C, 6 h) $La_{1-x}Ba_xMnO_3$ ($0.0 \le x \le 0.3$) samples, respectively. As-formed $La_{1-x}Ba_xMnO_3$ as well as calcined $La_{1-x}Ba_xMnO_3$ compounds show crystalline cubic phase. The XRD patterns of the as-formed samples with $x=0$ and 0.1 (Fig. 1(a) and (b)) show complete crystalline, impurity free phase with cubic symmetry, whereas for $x=0.2$ and 0.3 (Fig. 1(c) and (d)) show small impurity peak at $2\theta \approx 24°$ correspond to $BaCO_3$ [JCPDF No. 45-1471]. The formation of $BaCO_3$ phase might be due to the result of the reaction between BaO and CO_2 evolved during combustion process. On calcination at 900 °C for 6 h, $BaCO_3$ formed during combustion gets decomposed and hence all calcined barium doped manganites show cubic phase free from $BaCO_3$ impurity (Fig. 2(b)–(d)), whereas parent lanthanum manganites on calcination (900 °C, 6 h) transformed to rhombohedral phase. The strong oxidizing atmosphere, which exists during combustion reaction, leads to excess of Mn^{4+} (more than 34%) formation in these compounds and stabilizes cubic phase [20]. The broadness of XRD peaks indicates the nanocrystalline nature of the combustion-derived products. Crystallite sizes of the as-made and calcined powders were calculated from the broadening of the X-ray diffraction peaks using the Scherrer's formula [21], $S = K\lambda/\beta\cos\theta$, where K is

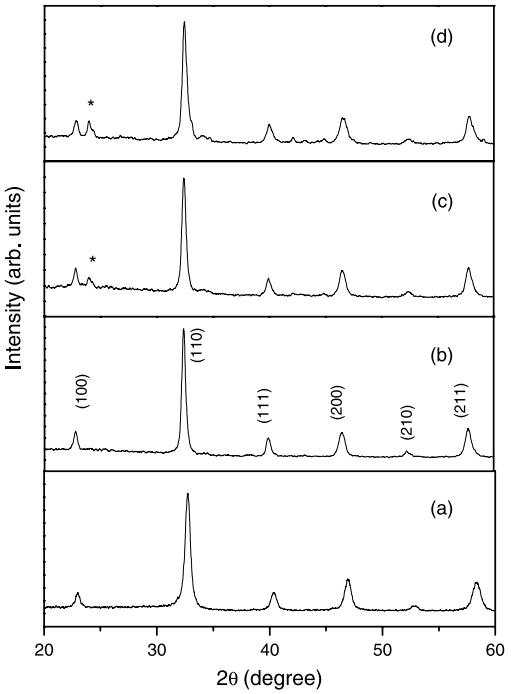

Fig. 1. PXRD patterns of as-formed $La_{1-x}Ba_xMnO_3$ ($0.0 \leq x \leq 0.3$) (*$BaCO_3$ impurity peaks): (a) $x=0.0$; (b) $x=0.1$; (c) $x=0.2$; and (d) $x=0.3$.

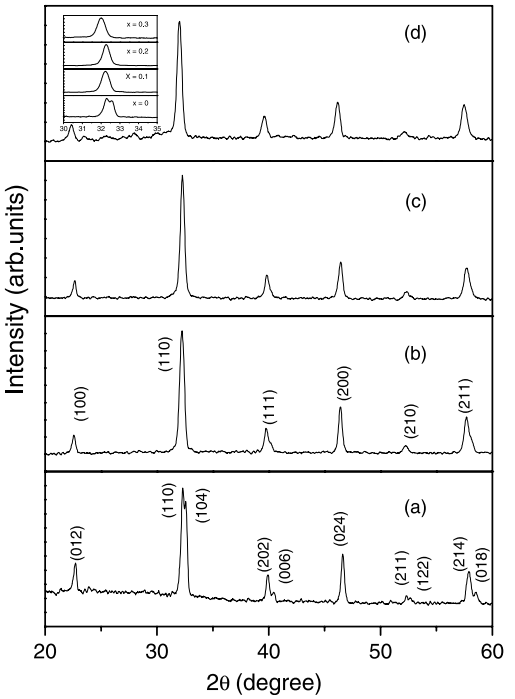

Fig. 2. PXRD patterns of calcined (900 °C, 6 h) $La_{1-x}Ba_xMnO_3$ ($0.0 \leq x \leq 0.3$) samples: (a) $x=0.0$; (b) $x=0.1$; (c) $x=0.2$; and (d) $x=0.3$. The inset shows the shift in (110) peak with x.

constant, λ is the wave length of Cu K_α radiation (1.541 Å) and β is the full width at half maxima (FWHM) of XRD peaks. In the present work, the crystallite sizes of the doped lanthanum manganites are in the range 33–45 nm. As the barium content increases in $La_{1-x}Ba_xMnO_3$, the diffraction peaks slightly shift to lower 2θ values, indicating that the lattice-parameters increase with the increase of barium doping level, which may be caused by larger ionic size of Ba^{2+}(1.61 Å) ion in comparison with La^{3+}(1.36 Å) ion. This shift also confirms the accommodation of Ba^{2+} ion into the lattice structure. The structure of the calcined (900 °C, 6 h) compounds was refined by Rietveld technique [22] using Fullprof suite program. Doped compounds are refined in cubic structure with *Pm*3*m* space group, whereas undoped calcined $LaMnO_3$ sample refined (hexagonal setting) in rhombohedral symmetry with *R*-3*c* space group. The composition, refined, structural, lattice parameters and *R*-factors are summarized in Table 1.

3.2. Scanning electron microscope

The surface morphology of $La_{1-x}Ba_xMnO_3$ ($0.0 \leq x \leq 0.3$) series was investigated by SEM. All combustion-derived samples are foamy products with large agglomerates of very fine particles. The foamy nature of combustion-derived samples can be attributed to large amount of gases evolved during combustion reaction. Fig. 3(a) shows SEM micrograph of as-formed $LaMnO_3$ sample and the size of the agglomerated particles are in the range 0.5–4.0 μm. Fig. 3(b) and (c) show micro photographs of as-formed and calcined $La_{0.7}Ba_{0.3}MnO_3$ (900 °C, 6 h) samples, respectively. It is observed that in doped manganites, the size of the primary particles in agglomerates is smaller compared to undoped manganites. The reduction in particle size with barium doping leads to increase in surface area and this is confirmed by surface area measurements. However, in calcined $La_{0.7}Ba_{0.3}MnO_3$ manganites, the particle size increases that leads to decrease in surface area of the sample.

3.3. Determination of Mn^{4+} concentration

The Mn^{4+} content is a crucial factor in determining the magnetic and transport properties of manganites [8,23,24]. The electron hopping between Mn^{3+} and Mn^{4+} is responsible for the relatively low resistivity as well as the ferromagnetism. In the present study, the Mn^{4+} content in as-formed and calcined $La_{1-x}Ba_xMnO_3$ ($0.0 \leq x \leq 0.3$) manganites is estimated from the iodometric titration [25]. It is found that the Mn^{4+} concentration in as-formed samples is 34, 36, 40 and 45% for $x=0.0$, 0.1, 0.2 and 0.3, respectively. Whereas, in calcined samples it reduces to 32, 34, 37 and 40%, the strong oxidizing atmosphere that exists during combustion reaction also leads to excess of Mn^{4+}

Table 1
Composition, lattice parameters, cell volume and *R*-factors of nanocrystalline $La_{1-x}Ba_xMnO_3$ samples (900 °C, 6 h)

Compounds	$LaMnO_3$	$La_{0.9}Ba_{0.1}MnO_3$	$La_{0.8}Ba_{0.2}MnO_3$	$La_{0.7}Ba_{0.3}MnO_3$
System	Rhombohedral	Cubic	Cubic	Cubic
Space group	*R*-3*c*	*Pm*3*m*	*Pm*3*m*	*Pm*3*m*
Lattice parameter (Å)	$a=5.505(4)$ $c=13.301(5)$ $\alpha=60.6°$ (2)	$a=3.891(4)$	$a=3.898(4)$	$a=3.91(5)$
Unit cell volume $(Å)^3$	58.184	58.924	59.244	59.325
La/Ba(1a)				
x	0.000	0.000	0.000	0.000
y	0.000	0.000	0.000	0.000
z	0.250	0.000	0.000	0.000
Mn(1b)				
x	0.000	0.500	0.500	0.500
y	0.000	0.500	0.500	0.500
z	0.000	0.500	0.500	0.500
O1(1c)				
x	0.458(24)	0.500	0.500	0.500
y	0.000	0.500	0.500	0.500
z	0.250	0.500	0.500	0.500
R_P	2.67	4.05	3.45	3.86
R_{WP}	3.48	5.49	4.61	4.94
R_{Brag}	2.71	4.44	3.58	5.60
R_F	4.03	3.66	2.64	3.99

content in these compounds, compared to the samples prepared by high temperature routes.

3.4. Measurement of surface area

The surface areas of the undoped and doped manganites have been determined by Braunauer, Emmet and Teller (BET) method using nitrogen as adsorbent gas [26]. It is interesting to observe that the surface area of $La_{1-x}Ba_xMnO_3$ ($0.1 \leq x \leq 0.3$) increases with barium doping, whereas it decreases on calcination. In calcined (900 °C, 6 h) barium doped as-formed samples, the surface of 12.5, 20.2, 26.0 and 37.8 m^2/g have been observed for $x=0.0$, 0.1, 0.2 and 0.3, respectively. This may be due to on increase in barium content, the fire retention time decreases and this leads to the formation of products with smaller grain size. As gaseous products liberated during combustion, the agglomerates disintegrate and more heat is carried away from the system, thereby hindering the particle growth, leads to high surface area [27,28]. The surface area of $LaMnO_3$ and $La_{0.7}Ba_{0.3}MnO_3$ manganites decreases with calcination as 24.0, 19.5, 18.3, 12.5, 0.5 and 58.5, 53.2, 39.6, 37.8, 2.2 m^2/g, respectively, at as-formed, 400, 650, 900 and 1200 °C. The decrease in surface area with calcination is due to an increase in particle size.

3.5. Fourier transform infrared spectroscopy

FTIR spectra of a series of as-formed and that of calcined (900 °C, 6 h) $La_{1-x}Ba_xMnO_3$ ($0.1 \leq x \leq 0.3$) samples show two characteristic IR bands. The band around 600 cm^{-1} corresponds to the stretching mode ν_s, which involves the internal motion of a change in length of the Mn–O bond; the band around 400 cm^{-1} corresponds to the bending mode ν_b, which is sensitive to a change in the Mn–O–Mn bond angle [29,30]. As formed samples show IR band at 1450cm^{-1} assignable to $BaCO_3$ [31] impurity and on calcination (at 900 °C for 6 h) this band disappears. The formation of $BaCO_3$ is also evidenced by PXRD.

3.6. Low temperature resistivity measurements

The electrical transport behaviour is experimentally studied by measuring resistivity as a function of temperature by means of standard four-probe method without an applied magnetic field. The variation of zero field resistivity of $La_{1-x}Ba_xMnO_3$ ($0.0 \leq x \leq 0.3$) pellets (sintered at 900 °C for 6 h) as a function of temperature down to 77 K is shown in Fig. 4. We observed that the samples studied in the present work show different resistivity behavior from that of single crystalline [32] material and also the samples prepared by ceramic route [33]. Hwang et al. [32] compared the magnetotransport property in polycrystalline samples with that in the single crystal. It was found that the polycrystalline compounds exhibited high resistivity values, which are far above those of single crystal, and a sharp drop of resistance in the low magnetic field. According to the experimental results, they attributed this to spin-polarized tunneling through an insulating grain boundary. The DE mechanism links the electronic transport to the magnetic

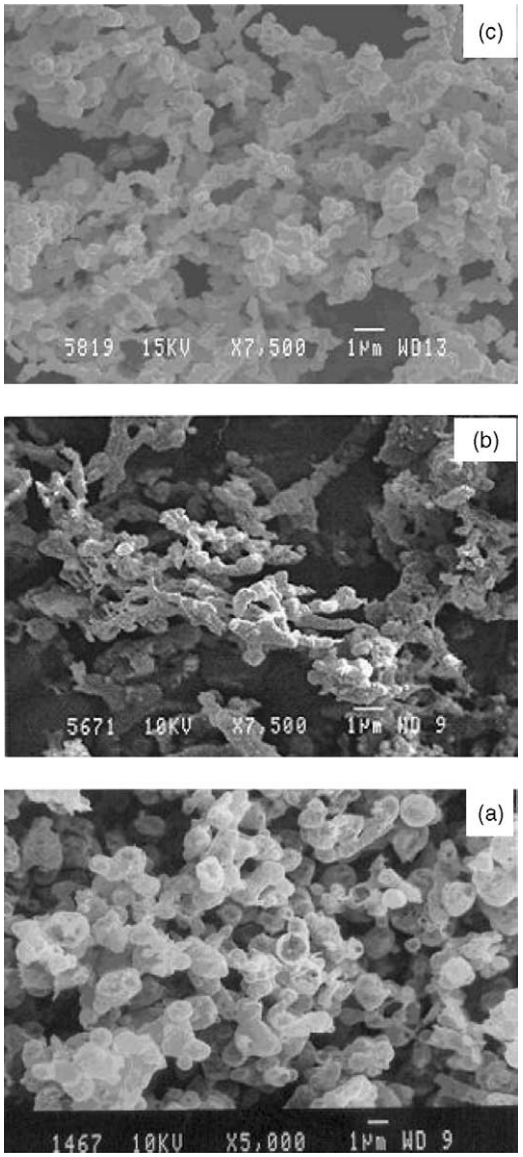

Fig. 3. SEM micrographs of (a) as-formed $LaMnO_3$; (b) as-formed $La_{0.7}Ba_{0.3}MnO_3$; and (c) calcined $La_{0.7}Ba_{0.3}MnO_3$ (900 °C, 6 h).

transition and describes the hopping of electrons in e_g orbitals between neighbouring Mn^{3+} and Mn^{4+} sites with strong on-site Hund's coupling through an O^{2-} ion. The electrons in these materials are able to move easily (enhancement in the ferromagnetic state) when the spins of the ions (Mn^{3+} and Mn^{4+}) are parallel and cannot move if they are antiparallel [34].

Doped lanthanum manganites with bigger grain size exhibit sharp metal–insulator transition. However, combustion derived samples show a broad transition due to nanocrystalline nature of the powders [35,36]. Studies on $La_{1-x}Ba_xMnO_3$, in the present work show distinct

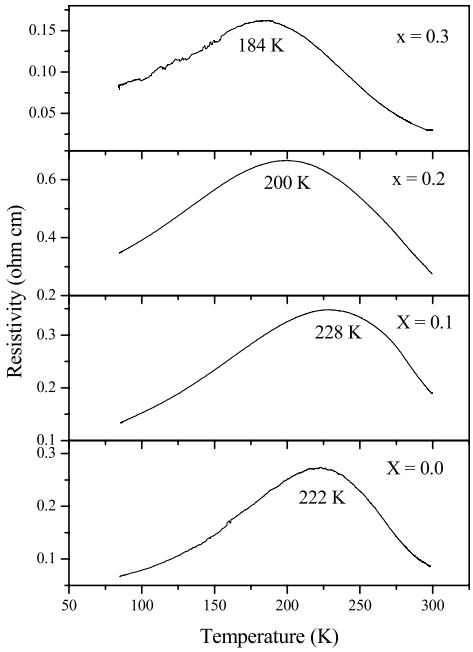

Fig. 4. Low temperature electrical resistivity of $La_{1-x}Ba_xMnO_3$ ($0.0 \leq x \leq 0.3$) samples.

resistivity maxima due to metal–insulator transition and exhibit T_{M-I} in the range 184–228 K. It is interesting to note that, as the barium content increases the T_{M-I} shifts to lower temperature side. The maximum T_{M-I} of 228 K is observed for $La_{0.9}Ba_{0.1}MnO_3$ sample. The observed T_{M-I} values for this sample found to be lower compared to the samples prepared via ceramic route [37] might be due to grain boundary effect.

The effect of grain size on magnetic, transport and structural properties of manganites have been studied by several investigators [38–40] which are attributed that the particles size, the doping level in lanthanum site, oxygen content and grain boundary effect play an important role in magnetic and electronic properties of these oxides. However, many controversial reports have also been reported in the literature pertaining to the effect of grain size on the magnetic properties of polycrystalline manganites. For instance Zhang et al. [39] studied the effect of grain size in $La_{0.85}Sr_{0.15}MnO_3$ and found that the magnetization and Curie temperature (T_C) decreases with increase in grain size. Sanchez et al. [38] have reported a contrary results, i.e. the decrease of T_C of $La_{.67}Ca_{0.33}MnO_3$ with decreasing grain size.

In the present study, we observed that the resistivity slightly increases with barium content up to $x=0.2$ and thereafter decreases. $La_{0.7}Ba_{0.3}MnO_3$ sample exhibit low resistivity at room temperature as well as at T_{M-I} because, this compound consists of high concentration of Mn^{4+} (40%). In presence of high concentration of Mn^{4+}, there is

formation of the maximum number of ferromagnetic clusters consist of Mn^{3+} and Mn^{4+} within a grain. The hopping of electron from Mn^{3+} to Mn^{4+} via oxygen is rapid and giving rise to relatively low resistivity for $La_{0.7}Ba_{0.3}MnO_3$ [41].

4. Conclusions

Nanocrystalline manganites of composition $La_{1-x}Ba_xMnO_3$ ($0.0 \leq x \leq 0.3$) have been synthesized by solution combustion route using corresponding metal nitrates as oxidizers and ODH as fuel. The time taken for the preparation is only few minutes ($\sim$5 min) and the synthesis temperature employed is lower than those currently used in conventional routes. This method also enables the formation of homogeneous and high surface area nanocrystalline powders of manganites. The as-formed manganites show crystalline cubic phase with impurity peak corresponds to $BaCO_3$. The stabilization of cubic phases in doped lanthanum manganites is due to substitution of Ba^{2+} in La^{3+} sites, resulting in higher Mn^{4+} content. The resistivity results showed that the barium doping level has a direct effect on the T_{M-I} and resistance of the samples. With increase in the barium doping level, T_{M-I} shifts to a lower temperature, which is encouraging. It is of interest to investigate CMR property of combustion derived nanocrystalline samples indeed, nanocrystalline manganites have a higher magnitude of the low field magnetoresistance as compared to ceramic samples and hence, further investigation on magnetic behavior and magnetoresistance studies are in progress.

Acknowledgements

G.T. Chandrappa gratefully acknowledges the financial support extended by DST (Government of India), New Delhi under the scheme Nanomaterials Science and Technology Initiative to carry out this work.

References

[1] A.P. Alivisatos Science 271 1996 933
[2] J.Z. Sun, et al., Appl. Phys. Lett. 69 (1996) 3266.
[3] S. Jin, et al., Science 264 (1994) 413.
[4] H.Y. Hwang, et al., Phys. Rev. Lett. 77 (1996) 2041.
[5] C. Zener, Phys. Rev. B 82 (1951) 403.
[6] P.W. Anderson, H. Hasegawa, Phys. Rev. 100 (1955) 675.
[7] P.G. De Gennes, Phys. Rev. 118 (1960) 141.
[8] G.H. Jonker, J.H. Van Santen, Physica 16 (1950) 337.
[9] E.L. Hueso, et al., J. Appl. Phys. 86 (1999) 3881.
[10] D.G. Lamas, et al., J. Magn. Magn. Mater. 241 (2002) 207.
[11] E. Vladimirova, et al., J. Mater. Sci. 36 (2001) 1481.
[12] G. Dezanneau, et al., Solid State Commun. 121 (2002) 133.
[13] J. Liu, et al., Mater. Res. Bull. 38 (2003) 817.
[14] S.T. Aruna, et al., J. Mater. Chem. 7 (1997) 2499.
[15] R.K. Sahu, et al., J. Mater. Sci. 36 (2001) 4099.
[16] S. Ekambaram, J. Alloys Compd. 390 (2005) L4.
[17] M. Verelst, et al., J. Solid State Chem. 104 (1993) 74.
[18] G. Gran, Anal. Chim. Acta 14 (1956) 150.
[19] G.T. Chandrappa, et al., J. Mater. Synth. Proc. 7 (1999) 273.
[20] G.H. Jonker, J. Phys. Chem. Solids 9 (1959) 165.
[21] H. Klug, L. Alexander, X-ray Diffraction Procedures, Wiley, New York, 1962. pp. 491.
[22] D.B. Wiles, R.A. Young, J. Appl. Crystallogr. 14 (1981) 149.
[23] E.O. Wollan, W.C. Koehler, Phys. Rev. 100 (1955) 545.
[24] R. Mahendiran, et al., Pramana 44 (1995) L393.
[25] R.N. Singh, et al., J. Solid State Chem. 132 (1998) 19.
[26] S. Brunauer, et al., J. Am. Chem. Soc. 66 (1938) 309.
[27] J. McKittrick, et al., Displays 19 (1999) 169.
[28] C.-C. Hwang, T.-Y. Wu, Mater. Sci. Eng. B 111 (2004) 197.
[29] F. Gao, et al., J. Alloys Compd. 347 (2002) 314.
[30] A. Arulraj, C.N.R. Rao, J. Solid State Chem. 145 (1999) 557.
[31] Z. Min-Guang, et al., J. Phys.: C 20 (1987) L917.
[32] H.Y. Hwang, et al., Phys. Rev. Lett. 77 (1996) 2041.
[33] H.L. Ju, et al., Phys. Rev. B 9 (1995) 6143.
[34] C. Zener, Phys. Rev. 81 (1951) 440.
[35] R. Mahesh, et al., Appl. Phys. Lett. 68 (1996) 2291.
[36] S.L. Yuan, et al., Solid State Commun. 121 (2002) 291.
[37] S.V. Trukhanov, J. Mater. Chem. 13 (2003) 347.
[38] R.D. Sanchez, et al., Appl. Phys. Lett. 68 (1996) 134.
[39] N. Zhang, et al., J. Phys.: C Matter 9 (1997) 4281.
[40] N. Zhang, et al., Phys. Rev. B 56 (1997) 8138.
[41] R. Mahendiran, et al., Solid State Commun. 99 (1996) 149.